Check for updates

Photodissociative decay pathways of the flavin mononucleotide anion and its complexes with tryptophan and glutamic acid†

Kelechi O. Uleanya, [iD] Cate S. Anstöter [iD] and Caroline E. H. Dessent [iD]*

Flavin mononucleotide (FMN) is a highly versatile biological chromophore involved in a range of biochemical pathways including blue-light sensing proteins and the control of circadian rhythms. Questions exist about the effect of local amino acids on the electronic properties and photophysics of the chromophore. Using gas-phase anion laser photodissociation spectroscopy, we have measured the intrinsic electronic spectroscopy (3.1–5.7 eV) and accompanying photodissociative decay pathways of the native deprotonated form of FMN, *i.e.* [FMN-H]⁻ complexed with the amino acids tryptophan (TRP) and glutamic acid (GLU), *i.e.* [FMN-H]⁻·TRP and [FMN-H]⁻·GLU, to investigate the extent to which these amino acids perturb the electronic properties and photodynamics of the [FMN-H]⁻ chromophore. The overall photodepletion profiles of [FMN-H]⁻·TRP and [FMN-H]⁻·GLU are similar to that of the monomer, revealing that amino acid complexation occurs without significant spectral shifting of the [FMN-H]⁻ electronic excitations over this region. Both [FMN-H]⁻·TRP and [FMN-H]⁻·GLU are observed to decay by non-statistical photodecay pathways, although the behaviour of [FMN-H]⁻·TRP is closer to statistical fragmentation. Long-lived FMN excited states (triplet) are therefore relatively quenched when TRP binds to [FMN-H]⁻. Importantly, we find that [FMN-H]⁻, [FMN-H]⁻·TRP and [FMN-H]⁻·GLU all decay predominantly *via* electron detachment following photoexcitation of the flavin chromophore, with amino acid complexation appearing not to inhibit this decay channel. The strong propensity for electron detachment is attributed to excited-state proton transfer within FMN, with proton transfer from a ribose alcohol to the phosphate preceding electron detachment.

1. Introduction

Electron-transfer processes within peptides and proteins are key steps in many biochemical reactions, including respiration and photosynthesis.[1] These events involve cofactors as the redox centres, but can also use amino acid radicals as intermediates.[2] Such events are challenging to characterize due to their short-lived nature, but are thought to be of particular importance in light-induced electron-transfer reactions.[3,4] Flavins are common cofactors in these chains, where their photoreduction by electron transfer from proximal tryptophan or tyrosine to an electronically excited flavin is believed to act as an efficient fluorescence quenching pathway.[5] Examples of such pathways include those active in cryptochrome, BLUF domain proteins and DNA photolyases.[6] Given the wide biochemical importance of these

systems, they have been extensively investigated by static and ultrafast photochemical methods.[7] However, interpretation of the results obtained is still highly challenging, particularly given the difficulties of applying computational chemistry to a system that is conformationally complex, alongside the demands of modelling coupled electron-transfer processes and electronic excited states.[7]
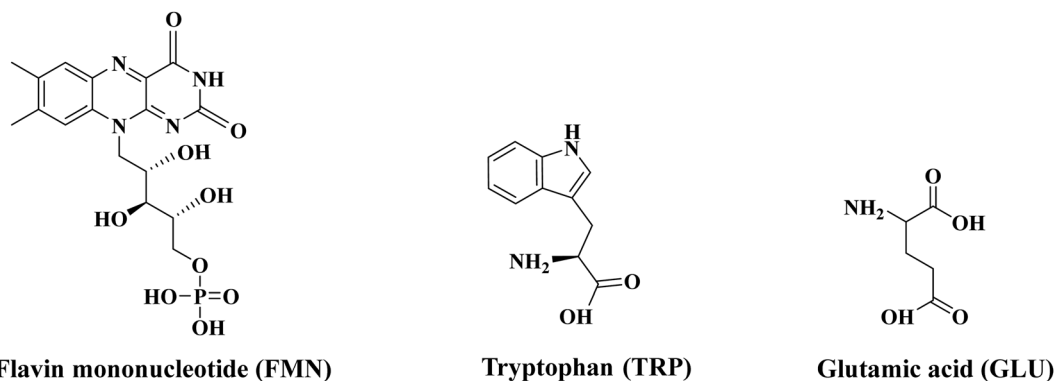
In this work, we present the first *in vacuo* electronic laser spectroscopy of a flavin molecule bound directly in a molecular complex to the amino acid tryptophan (TRP), which is a key amino acid in photoredox active centres in flavin containing proteins.[8] We aim to investigate the potential of such systems as prototypes for obtaining novel biochemical insights into flavin photochemistry, and obtain benchmarking data to evaluate the applicability of high-level computational chemistry approaches to flavin–amino acid structures. We have selected flavin mononucleotide (FMN) as the flavin molecule for this work, and study it as its native, singly-deprotonated form, where deprotonation is expected to occur at the phosphoric acid group ($pk_a \sim 2$).[9,10] In addition, we have chosen to study a complex of FMN with glutamic acid (GLU), as a prototype

Department of Chemistry, University of York, Heslington, York, YO10 5DD, UK.
E-mail: caroline.dessent@york.ac.uk

This journal is © the Owner Societies 2023

Phys. Chem. Chem. Phys., 2023, **25**, 30697–30707 | **30697**

Scheme 1 Schematic diagram of the structures of flavin mononucleotide (FMN), tryptophan (TRP) and glutamic acid (GLU).

simple, non-aromatic amino acid that is not generally involved in flavin photoredox proteins. Scheme 1 illustrates the individual structures of FMN, TRP and GLU. Since negatively charged systems are studied in this work, we are able to investigate how electron detachment competes with molecular fragmentation following photoexcitation. This is an important aspect of the fundamental photochemistry of flavins given their role as photoredox species. By studying the FMN monomer, and the amino acid complexes, we are able to measure the extent to which a bound amino acid can quench electron detachment from the flavin and determine whether photoinitiated electron-transfer from the flavin to these amino acids occurs.

Experiments in this work were performed *via* laser-interface mass spectrometry (LIMS), which provides the gas-phase absorption spectra *via* photodepletion action spectroscopy, along with the spectroscopic production profiles of any ionic photofragments produced following photoexcitation.[11,12] We combine our LIMS measurements with higher-energy collisional dissociation (HCD) measurements that reveal the ionic fragmentation pattern for the ground electronic state of the system under study.[13] This provides information on whether photofragmentation follows a statistical or non-statistical route, and hence provides insight into the photodynamics of decay.[14,15] (Further information on the insight that can be obtained from identifying statistical *versus* non-statistical routes in photodissociation can be found in ref. 16.)[16]

Giacomozzi and co-workers have studied the non-statistical fragmentation of photoactivated flavin mononucleotide anions recently using a custom-built instrument, the SepI accelerator mass spectrometer at Aarhus University.[17] They found that [FMN-H]$^-$ decomposes largely through non-statistical fragmentation pathways following photoexcitation between 300–500 nm. Preliminary measurements were also presented on the complex of [FMN-H]$^-$ with betaine to probe whether the electronic transitions display intramolecular charge-transfer character. The measurements we present here complement this earlier study as our instrument measures the production of photofragments over an extended timescale (typically up to 0.1 ms)[11] that is longer than biochemical decay processes to provide a complete picture of the photofragments produced.[12] Our accompanying HCD measurements provide further fundamental information for understanding the nature of the photodecay mechanisms displayed by the

complexes studied here.[13] Furthermore, since our experiment allows us to measure the electron detachment profile of a system we can obtain insight into the propensity for an anion to undergo electron detachment *versus* fragmentation following photoexcitation.[18,19]

Over the last five years, a growing number of flavin molecule ions and complexes have been investigated *in vacuo* using laser (IR and UV-VIS) photodissociation spectroscopy, including alkali metal-flavin (*e.g.* riboflavin and lumiflavin) clusters,[20,21] and protonated and deprotonated flavin molecules.[17,22–26] These studies have provided important new fundamental information on the spectroscopy and photochemistry of relatively simple flavin systems. We aim here to build on these recent studies by increasing the complexity and biological relevance of system to be investigated. Such measurements are part of wider advances employing gas-phase laser spectroscopy to advance our fundamental understanding of biomolecular systems.[27–33]

A very wide range of physical methods have been applied to study the condensed phase photophysics of flavins, both for free flavin moieties and flavoprotein photoreceptors.[7,34] A recent review by Kar *et al.* provides a useful overview of the state of knowledge on the broad field of flavin electronic structure that provides further background to the work presented here.[35] Readers may also be interested in the role of solvent in the dynamical process linked to flavin photoexcitation; ref z provides for further background on that point.[36]

2. Experimental method

FMN (70% purity), TRP (98% purity) and GLU (99% purity) were purchased from Sigma Aldrich and was used without further purification. HPLC-grade ethanol was purchased from Fisher Scientific, Inc. (Pittsburgh, PA, USA) and again used as received.

2.1 Laser-interfaced mass spectrometry

The experiment has been described in-full previously.[11,12] Briefly, gas-phase UV photodissociation experiments were conducted in an AmaZon SL dual funnel electrospray ionization quadrupole ion trap (ESI-QIT) mass spectrometer (Bruker Daltonics Inc.), which was modified to allow for laser-interfaced

30698 | *Phys. Chem. Chem. Phys.*, 2023, **25**, 30697–30707

This journal is © the Owner Societies 2023

mass spectrometry. Solutions of FMN (1.0×10^{-5} mol dm^{-3} with NH$_3$ (0.4%) added to aid ionization) in EtOH were introduced to the mass spectrometer using typical instrumental parameters: nebulizing gas pressure of 10.0 psi, an injection rate of 0.33 mL h^{-1}, a drying gas flow rate of 8.0 L min^{-1}, a capillary temperature of 160 °C. To form the amino acid–flavin complexes, 1 : 1 mixtures of FMN and the amino acids were combined, with both solutions being 1.0×10^{-5} mol dm^{-3}.

Ions were mass selected and isolated in the ion trap prior to UV laser irradiation. UV photons were produced with a 10 Hz Nd:YAG (Surelite™) pumped OPO laser (Horizon™), providing ∼0.2–1.0 mJ across the range 400–218 nm. Laser step sizes of 2 nm were used. Photofragmentation experiments were conducted with a set ion accumulation time of 10 ms and a corresponding fragmentation time of 100 ms, allowing for each mass-selected ion packet to interact with one laser pulse. The laser beam diameter is ∼2 mm in the ion interaction region of the ion trap. When fluorescence is negligible, UV-excited gaseous ions fragment upon excited-state relaxation, yielding an action absorption spectrum by photodepletion.

2.2 Analysis

Photodepletion (PD) was measured as a function of scanned wavelength, with the photofragment production (PF) recorded simultaneously at each corresponding wavelength.[37] As described by eqn (1a) and (1b), Int$_{OFF}$ and Int$_{ON}$ represent the parent ion intensities with laser off and on, respectively; Int$_{FRAG}$ is the photofragment intensity with the laser on; λ is the excitation wavelength (nm); and P is the tuneable laser pulse energy (mJ).

$$\text{Photodepletion intensity} = \frac{\ln\left(\dfrac{\text{Int}_{OFF}}{\text{Int}_{ON}}\right)}{\lambda \times P} \qquad (1a)$$

$$\text{Photofragment production intensity} = \frac{\ln\left(\dfrac{\text{Int}_{FRAG}}{\text{Int}_{OFF}}\right)}{\lambda \times P} \qquad (1b)$$

The photodepletion intensities were taken from an average of three repeat runs at each wavelength studied. We note that photofragment ions with $m/z < 50$ are not detectable within our mass spectrometer since low masses fall outside of the mass window of the ion trap.

2.3 Higher-energy collisional dissociation

Experiments were performed in a Thermo Fisher Orbitrap Fusion™ mass spectrometer, as described previously.[13] (We are not able to provide a center-of-mass collision energy that corresponds to a percentage HCD in our experiments, as we perform the experiments in a commercial mass spectrometer, which does not allow sufficient collision cell pressure variability to allow calibration. In our earlier work,[13] we were able to link our results on deprotonated adenosine monophosphate to those of Ho and Kebarle,[38] who had obtained an absolute measurement of center of mass collision energy through absolute calibration of their system for the same ion. This allowed us to obtain an approximate calibration of the HCD fragmentation

curves and conclude that the 4–6 eV energy range (photon energy) corresponds to the 20–38% range on the HCD fragmentation plots.)

The following settings were used for the HCD experiments: the syringe was operated at a flow rate of 3 μL min^{-1} and with the following settings: MS2 scan isolation mode, ion trap; detector type, ion trap; positive ion spray voltage (3500 V); RF lens (60%); normalized AGC target (100%); maximum injection time (100 ms); ion transfer tube temperature (275 °C); and vaporizer temperature (20 °C). For the MS scan in this instrument, the settings were as follows: detector type, Orbitrap; positive ion spray voltage (3200 V); RF lens (45%); normalized AGC target (100%); and maximum injection time (100 ms).

2.4 Calculations

Schrodinger's MacroModel with mixed Monte Carlo torsional and low-mode sampling parameters were employed to conduct conformational molecular dynamics searches to generate possible conformers of the [FMN-H]$^{-}$·TRP and [FMN-H]$^{-}$·GLU clusters.[39] Possible conformers were energy gradient minimized with the OPLS3e force-field. Single-point energies were then performed at the PBE0/6-311++G level of theory.

3. Results and discussion

3.1 Photodepletion spectra

Fig. 1a displays the photodepletion (gas-phase absorption) spectra of singly deprotonated FMN, $i.e.$ [FMN-H]$^{-}$, acquired from 3.1–5.7 eV (400–218 nm). While related data has been published by Giacomozzi $et~al.$ recently,[17] the [FMN-H]$^{-}$ spectrum was reacquired here to allow a direct comparison with the cluster spectra that are the main focus of this work.

Three regions of absorption for [FMN-H]$^{-}$ are evident over the spectral region (labelled I–III), with the absorption onset occurring around 3.2 eV. Band I is a relatively weak broad band and is observed across the visible region, centred around 3.6 eV. This band decreases in intensity above 3.9 eV and approaches a baseline level by 4.1 eV. Band II appears strongly between 4.2–5.2 eV, displaying a maximum at 4.75 eV, with the rising edge of band III is evident above 5.3 eV. The photodepletion spectra of the complexes (Fig. 1b and c), [FMN-H]$^{-}$·TRP and [FMN-H]$^{-}$·GLU, are similar to that of the monomer with the λ_{max} of bands I and II occurring at 3.52 and 4.71 eV, respectively for [FMN-H]$^{-}$·TRP, and at 3.73 and 4.76 eV for [FMN-H]$^{-}$·GLU. The fact that the photodepletion spectra of the two complexes, and the monomer, all appear very similar is striking, as complexation of a molecule to a chromophore will generally result in a significant spectral shift. One explanation of the absence of spectral shifts in the spectra shown in Fig. 1 may be that the amino acids bind to the phosphate chain of FMN and are therefore distant from the alloxazine chromophore. This will be discussed in more detail below. Finally, we note that neutral tryptophan has an absorption band between 300–250 nm, so that [FMN-H]$^{-}$·TRP photodepletion observed
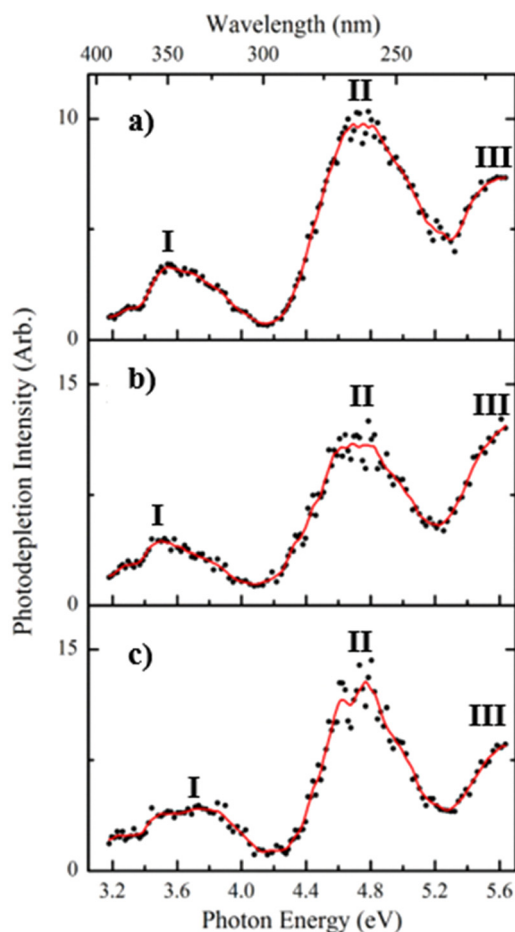
Fig. 1 Gas-phase photodepletion (action absorption) spectra of (a) [FMN-H]⁻, (b) [FMN-H]⁻·TRP and (c) [FMN-H]⁻·GLU across the range 3.1–5.7 eV. The solid lines are five point adjacent averages of the data points.

across that range may include depletion associated with excitation of the tryptophan chromophore.

The bands observed in the spectra presented in Fig. 1 can be related to the known electronic states of flavins. In brief, flavins display singlet excited states at approximately 2.85, 3.76 and 4.7, with triplet states occurring at around 3.1 and 4.3 eV. Bands I and II can therefore be assigned to excitation of the second and third singlet states of [FMN-H]⁻, with the first and second triplet states, respectively, being accessible *via* intersystem crossing from these bands, respectively.[40]

Laser-energy dependent photodepletion measurements were conducted for [FMN-H]⁻, with laser energies above ∼0.4 mJ being associated with multiphoton processes (Section S1, ESI†). The observation of multiphoton processes at higher laser energies is consistent with similar measurements conducted on this system previously.[17] Laser-energy dependent photodepletion measurements were also attempted for the clusters, but were challenging due to the relatively lower ion intensities of the precursor complexes. It is reasonable to assume that at sufficiently high laser energies, similar multiphoton effects will be present for the clusters. For the spectra presented here, we reduced the laser energy to 0.20 mJ to conduct the measurements

on [FMN-H]⁻ in a single-photon regime, obtaining photodepletion ∼35% of the precursor ion intensity. A similar photodepletion intensity was employed for the measurements on the complexes (35% of precursor ion intensity) so that the cluster spectra also predominantly result from single-photon excitations.

While the photodepletion spectra of [FMN-H]⁻, [FMN-H]⁻·TRP and [FMN-H]⁻·GLU are evidently very similar, the photodepletion cross section masks the detail of the excited state decay pathways. This is revealed much more clearly by measuring the spectral profiles of the photofragments produced following excited-state decay.[12] We therefore turn to exploring the [FMN-H]⁻, [FMN-H]⁻·TRP and [FMN-H]⁻·GLU photofragment ions and their production spectra in the next section.

3.2 Photofragmentation

Fig. 2 displays the photofragment ions produced for each of these species following photoexcitation at 4.73 eV, the region of the band II peak (maximum photodepletion). Photofragmentation of
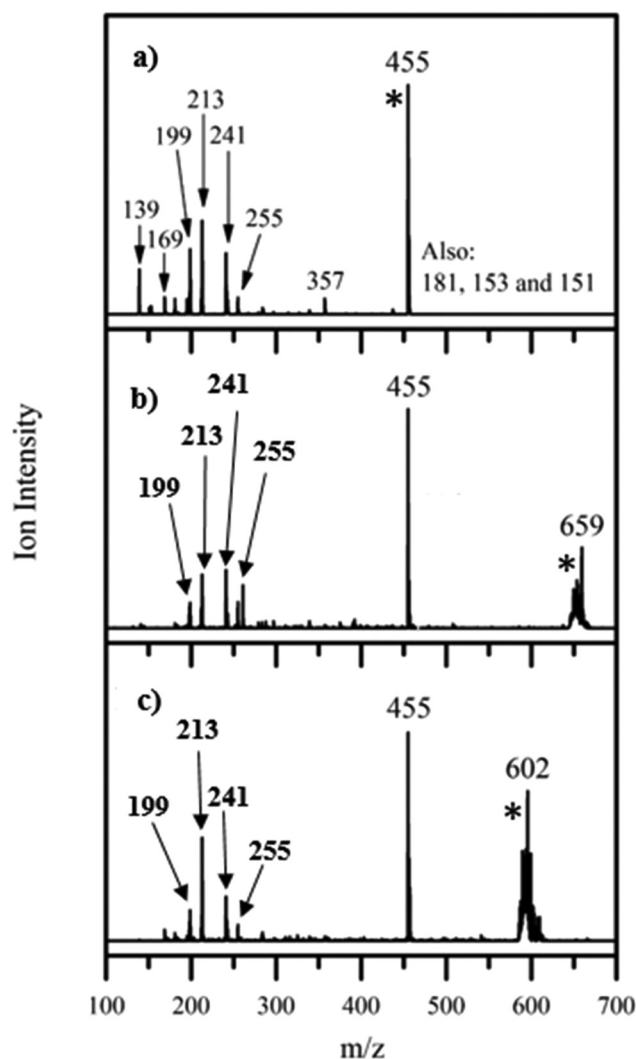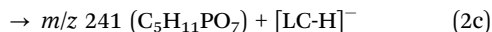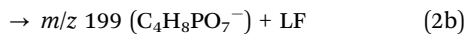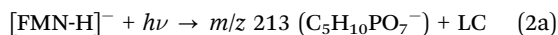

Fig. 2 Photofragment difference (laser$_{ON}$ − laser$_{OFF}$) mass spectra for (a) [FMN-H]⁻, (b) [FMN-H]⁻·TRP and (c) [FMN-H]⁻·GLU excited at 4.73 eV. [*] indicates the photodepleted parent ion.

30700 | *Phys. Chem. Chem. Phys.*, 2023, **25**, 30697–30707

This journal is © the Owner Societies 2023

[FMN-H]$^-$ occurs into numerous channels, with the most intense fragments being m/z 213, 199, and 241. These ions correspond to the following three dissociative pathways, where LC and LF are the smaller flavin molecules, lumichrome and lumiflavin, respectively:

$$[FMN\text{-}H]^- + h\nu \rightarrow m/z\ 213\ (C_5H_{10}PO_7{}^-) + LC \quad (2a)$$

$$\rightarrow m/z\ 199\ (C_4H_8PO_7{}^-) + LF \quad (2b)$$

$$\rightarrow m/z\ 241\ (C_5H_{11}PO_7) + [LC\text{-}H]^- \quad (2c)$$

Thus, the dominant photofragmentation pathways involve rupture of the isoalloxazine chromophore-ribose phosphate chain, with or without retention of the lumiflavin methyl group. The appearance of the m/z 213 and 241 pair of photoproducts is interesting, as they suggest that the precursor ion structure may involve an ion where the phosphate binds close to the alloxazine ring, allowing facile charge exchange during fragmentation.

A list of the most intense photofragments of [FMN-H]$^-$ observed at 4.73 eV is given in Table 1, with their photofragmentation production spectra being displayed in Fig. S3 (ESI†). There is good agreement between the photofragments we observe and those seen by Giacomozzi *et al.* upon 450 nm photoexcitation, particularly with respect to the major intensity photofragments.[17] The major photofragments are also structurally similar to those observed upon photoexcitation of the related, deprotonated riboflavin ion across 2.0–5.74 eV.[22] (The riboflavin structure lacks the phosphate group of FMN.)

Fig. 2b displays the photofragments observed upon photoexcitation of the [FMN-H]$^-$·TRP complex at 4.73 eV (peak of band II), with a list of the photofragments being given in Table 2 along with assignments. The most intense photofragment observed is m/z 455, *i.e.* [FMN-H]$^-$, which is the product of upon cluster fission, with the other major fragments (m/z 241, 213, 199 and 255) having been observed for the [FMN-H]$^-$ monomer. The photofragmentation mass spectrum for the [FMN-H]$^-$·GLU complex, again obtained at 4.73 eV, is displayed in Fig. 2c, and is similar to that of [FMN-H]$^-$·TRP, with m/z 455

Table 1 Fragments of [FMN-H]$^-$ (m/z 455) produced upon laser photo-dissociation (PF) at 4.73 eV and higher-energy collisional dissociation (HCD) between 0–42%[a]

Fragments	HCD	Photo fragments	Neutral loss	Fragment identity	Neutral identity
79	✓	X	376	PO$_3{}^-$	RF
97	✓	X	358	H$_2$PO$_4{}^-$	RF-H$_2$O
139	✓	✓	316	C$_2$H$_4$PO$_5{}^-$	LF + 2(H$_2$CO)
159	✓	X	296	C$_2$H$_8$PO$_6{}^-$	LC + C$_3$H$_2$O
169	X	✓	286	C$_3$H$_6$PO$_6{}^-$	FMFH$_2$
181	✓	✓	274	C$_4$H$_6$PO$_6{}^-$	LF + H$_2$O
199	✓	✓	256	C$_4$H$_8$PO$_7{}^-$	LF
213	✓	✓	242	C$_5$H$_{10}$PO$_7{}^-$	LC
241	✓	✓	214	[LC-H]$^-$	C$_5$H$_{11}$PO$_7$
255	✓	✓	200	[LF-H]$^-$	C$_4$H$_9$PO$_7$
357	✓	✓	98	[RF-H$_2$O-H]$^-$	H$_3$PO$_4$
375	✓	X	80	[RF-H]$^-$	HPO$_3$
412	✓	X	43	[FMN-HCNO]$^-$	HCNO
437	✓	✓	18	FMN-H$_2$O	H$_2$O

[a] RF = riboflavin, LC = lumichrome, LF = lumiflavin, FMFH$_2$ = formylmethylflavin.

Table 2 Fragments of [FMN-H]$^-$·TRP (m/z 659) produced upon laser photodissociation (PF) at 4.73 eV and higher-energy collisional dissociation (HCD) between 0–8.5%[a]

Fragments	HCD	Photo fragments	Neutral loss	Fragment identity	Neutral identity
139	X	✓	520	C$_2$H$_4$PO$_5{}^-$	LF + 2(H$_2$CO) + TRP
169	X	✓	490	C$_3$H$_6$PO$_6{}^-$	FMFH$_2$ + TRP
199	X	✓	460	C$_4$H$_8$PO$_7{}^-$	LF + TRP
213	X	✓	446	C$_5$H$_{10}$PO$_7{}^-$	LC + TRP
241	X	✓	418	[LC-H]$^-$	C$_5$H$_{11}$PO$_7$ + TRP
255	X	✓	404	[LF-H]$^-$	C$_4$H$_9$PO$_7$ + TRP
375	X	✓	384	[RF-H]$^-$	HPO$_3$ + TRP
392	X	✓	267	[FMN-H$_2$O]$^-$	H$_2$O + TRP
455	✓	✓	204	[FMN-H]$^-$	TRP

[a] RF = riboflavin, LC = lumichrome, LF = lumiflavin, FMFH$_2$ = formylmethylflavin.

Table 3 Fragments of [FMN-H]$^-$·GLU (m/z 602) produced upon laser photodissociation (PF) at 4.73 eV and higher-energy collisional dissociation (HCD) at 0–8.5%[a]

Fragments	HCD	Photo fragments	Neutral loss	Fragment identity	Neutral identity
199	X	✓	403	C$_4$H$_8$PO$_7{}^-$	LF + GLU
213	X	✓	389	C$_5$H$_{10}$PO$_7{}^-$	LC + GLU
241	X	✓	361	[LC-H]$^-$	C$_5$H$_{11}$PO$_7$ + GLU
255	X	✓	347	[LF-H]$^-$	C$_4$H$_9$PO$_7$ + GLU
455	✓	✓	147	[FMN-H]$^-$	GLU

[a] LC = lumichrome, LF = lumiflavin.

being the dominant photofragment (*i.e.* [FMN-H]$^-$) along with m/z 241, 213, 199 and 255. Table 3 lists the fragments observed for [FMN-H]$^-$·GLU. We note that the deprotonated amino acid is not observed as a photofragment from either complex.

Fig. S4 and S5 (ESI†) display the full photofragmentation spectra of [FMN-H]$^-$·TRP and [FMN-H]$^-$·GLU across 3.1–5.7 eV, and reveal how photofragment production varies for the two complexes across the spectral range investigated. For [FMN-H]$^-$·TRP, the m/z 241, 213 and 199 fragments' production profiles closely match that of band I. The m/z 455 fragment is produced most strongly through band I, but with a profile that differs from those of the m/z 241, 213 and 199 group. For [FMN-H]$^-$·GLU, the m/z 241, 213 and 199 group are again produced with a profile that follows band I. However, the fragment production across band II is more complicated, with m/z 455 being the most intense fragment, but not being produced with a profile that matches the photodepletion band. These variations reflect differences in the excited states and available decay pathways of the three systems studied, and will be discussed further in Section 3.5.

3.3 Photofragmentation *versus* electron detachment and electron transfer

For simple anionic systems, *i.e.* ones that are rigid, photofragmentation will occur in competition with electron detachment at photon energies above the electron detachment threshold.[41,42] In our experiment, we can estimate the extent of electron detachment by assuming that any photodepletion that is not associated

with ionic-fragment production is associated with electron loss.[18,19] The electron production spectra for [FMN-H]⁻, [FMN-H]⁻·TRP and [FMN-H]⁻·GLU (Fig. S6, ESI†) show that electron detachment is the dominant decay channel with > 80% of all observed photodecay mechanisms channelling into electron detachment. This is intriguing since the electron detachment energy of the phosphate moiety of [FMN-H]⁻ is expected to be above ∼ 5 eV,[43,44] so that electron loss cannot be attributed to direct detachment below such energies. (However, the electron detachment yield can be seen to increase significantly above 5.4 eV where direct detachment is likely to occur.) Furthermore, the electron production spectra for [FMN-H]⁻, and the complexes (Fig. S6, ESI†) show that the electron detachment profiles closely match the photodepletion spectra. This is important as it allows us to conclude that electron detachment is strongly coupled to electronic excitation of the flavin chromophore.[41] We will discuss this point further in Section 4.

No photoinitiated electron transfer is observed from [FMN-H]⁻ to either of the amino acids studied here. We have been able to observe intracluster electron transfer from halide ions to a range of molecules in previous work,[41,45–47] where dipole-bound excited states have acted as doorway states for electron transfer within the cluster. The absence of electron transfer for the flavin clusters *via* such mechanisms here may be attributed to a low (conformational) dipole moment of the amino acid within the cluster, or to relatively weak Frank–Condon factors from the relatively delocalized phosphate anion to any existing dipole-bound excited state.[48]

3.4 Higher-energy collisional dissociation

To probe the collisional activated fragmentation pathways of [FMN-H]⁻, [FMN-H]⁻·TRP and [FMN-H]⁻·GLU in their electronic ground states, higher-energy collisional dissociation (HCD) was employed. Fig. 3 displays the HCD curves for the major fragments observed for each of these species. HCD measurements are important for interpreting ionic photodissociation measurements as they allow for the identification of primary and secondary products, formed when a precursor species fragments at high internal energy.[13] They are also important as any photofragment ions not observed in HCD can be identified as purely photochemical products.

The HCD results for [FMN-H]⁻ are presented in Fig. 3a, clearly showing that the *m/z* 97 ion ($H_2PO_4^-$) is the most intense fragment across the majority of the range studied. (At the very lowest energies, the *m/z* 255 fragment is most intense, albeit with very low intensity.) The next most intense fragments are *m/z* 79, 199 and 255. At higher collisional energies (> 28%), the relative intensity of *m/z* 79 (PO_3^-) can be seen to increase significantly, indicating that this fragment is a secondary fragment, particularly of the higher mass fragments. Giacomozzi *et al.* have previously measured collisional dissociation of [FMN-H]⁻ in the SepI accelerator mass spectrometer at low and high collision energies.[17] In their high-energy collision measurement, they observe the *m/z* 97 ion as the dominant fragment ion, with only *m/z* 79 and *m/z* 241 as additional ionic fragments. At low collision energy (multiple few-eV collisions in ion trap), they observe the
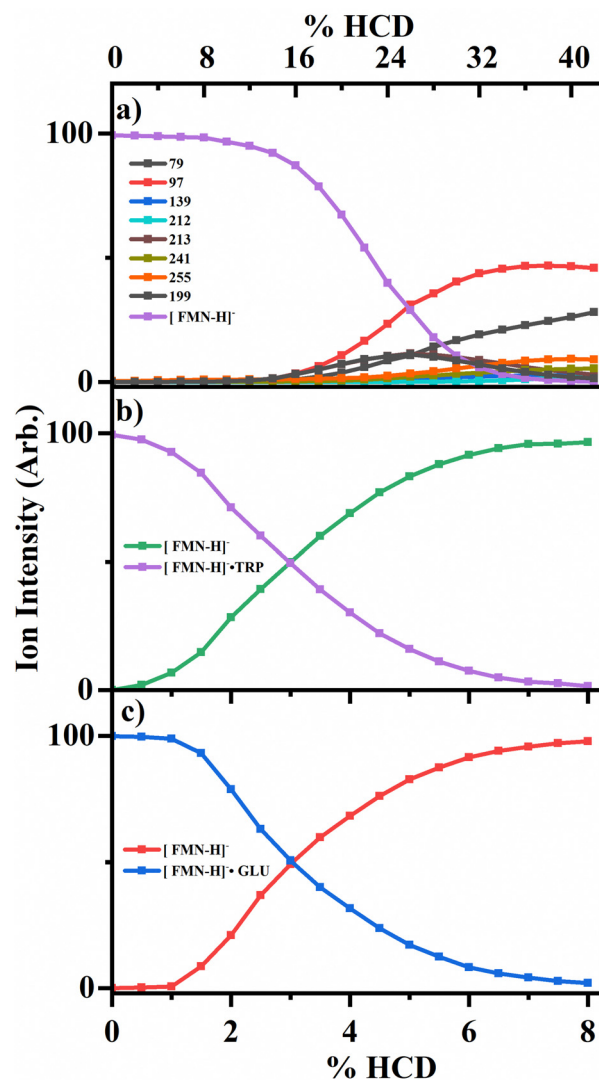

Fig. 3 Percent ion intensity of the HCD fragments of (a) [FMN-H]⁻ (from 0–42% HCD energy) (b) [FMN-H]⁻·TRP and (c) [FMN-H]⁻·GLU (from 0–8.5% HCD energy). The solid lines are three point averages of the data points.

m/z 241 ion as the dominant fragment, with the *m/z* 97 ion as the second most intense fragment, with *m/z* 255, 213, and 79 also present in significant quantities. This is consistent with their high-collision energy measurement being more energetic than the maximum HCD energy studied in this work. While the two measurements are complementary, the HCD data presented in Fig. 3 give a fuller picture of how fragment ions vary continuously with respect to one another over the laser excitation energies employed here.[13]

Fig. 3b and c display the HCD results for the two complexes, [FMN-H]⁻·TRP and [FMN-H]⁻·GLU, showing that the clusters undergo cluster fission with ejection of the amino acid as the dominant process at all collisional energies, *i.e.*

$$[FMN-H]^- \cdot TRP \rightarrow [FMN-H]^- + TRP \qquad (3a)$$

$$[FMN-H]^- \cdot GLU \rightarrow [FMN-H]^- + GLU \qquad (3b)$$

30702 | *Phys. Chem. Chem. Phys.*, 2023, **25**, 30697–30707

This journal is © the Owner Societies 2023

Similar results have been seen previously in HCD and lower-energy CID of other ionic molecular complexes,[41,49] and are consistent with collisional energy being funnelled into fragmenting the relatively weak intermolecular bonds. It is notable in this context that the complexes are completely dissociated at significantly lower HCD energies than the monomer. Tables 1–3 include a list of the observed HCD fragments, with assignments.

In summary, the HCD measurements indicate that ionic fragmentation of the ground electronic states of $[FMN-H]^-$, $[FMN-H]^-\cdot TRP$ and $[FMN-H]^-\cdot GLU$ are straightforward. $[FMN-H]^-$ fragments predominantly with loss of the $H_2PO_4^-$ ion, with the m/z 79, 199 and 255 ions also being observed at significant intensities, and m/z 79 (PO_3^-) growing in intensity as collisional energy increases. Both complexes dissociate solely *via* cluster fission and production of $[FMN-H]^-$. We next turn to comparing the photofragmentation and HCD fragmentation patterns to gain insight into the photodissociation dynamics, and assess whether complexation affects the photodynamics.

3.5 Comparison of photofragmentation and higher-energy collisional dissociation of $[FMN-H]^-$, $[FMN-H]^-\cdot TRP$ and $[FMN-H]^-\cdot GLU$

From the data presented in Sections 3.2 and 3.3, it is evident that the ionic fragments observed upon photoexcitation of $[FMN-H]^-$ at 4.73 eV do not match those observed in the HCD measurements with photofragmentation being dominated by production of m/z 213, 199, and 241 while collisional dissociation leads dominantly to production of m/z 97, along with m/z 79, 199 and 255. Furthermore, the photofragment profiles vary significantly with photon energy (Fig. S2, ESI†). These observations are all consistent with non-statistical photodecay dynamics operating for the $[FMN-H]^-$ monomer. (Non-statistical decay is associated with dissociation occurring directly from the excited state without the involvement of a conical intersection to return the system to a near-starting point geometry. In non-statistical decay, the photofragments obtained will be notably different in their identities and relative intensities from the ground electronic state fragments seen from HCD.[14,15,50] Further information on the insight that can be obtained from identifying statistical *versus* non-statistical routes in photodissociation can be found in ref. 50.)

For ease of comparison, Fig. 4 presents a selection of plots which compare HCD fragment production with photofragment production for the $[FMN-H]^-$ monomer. In these plots, we have selected HCD energies that should be approximately equivalent to the photon energies employed. We emphasise that this is an approximation, as it is not able to straightforward to calibrate the HCD energies, but our previous work on deprotonated adenosine triphosphate allows us to make the approximate qualitative comparison we employ here.[13] The data displayed in Fig. 4 very clearly illustrate that the photofragment intensities do not mirror those obtained from HCD. Focusing on the key data for the band I and band II regions (Fig. 4A and B), the photofragments m/z 199, 213 and 241 can be seen to be significantly more intense than would be expected from the HCD fragments over the band I region (Fig. 4A) while production of m/z 241 ion in particular increasing for the band II
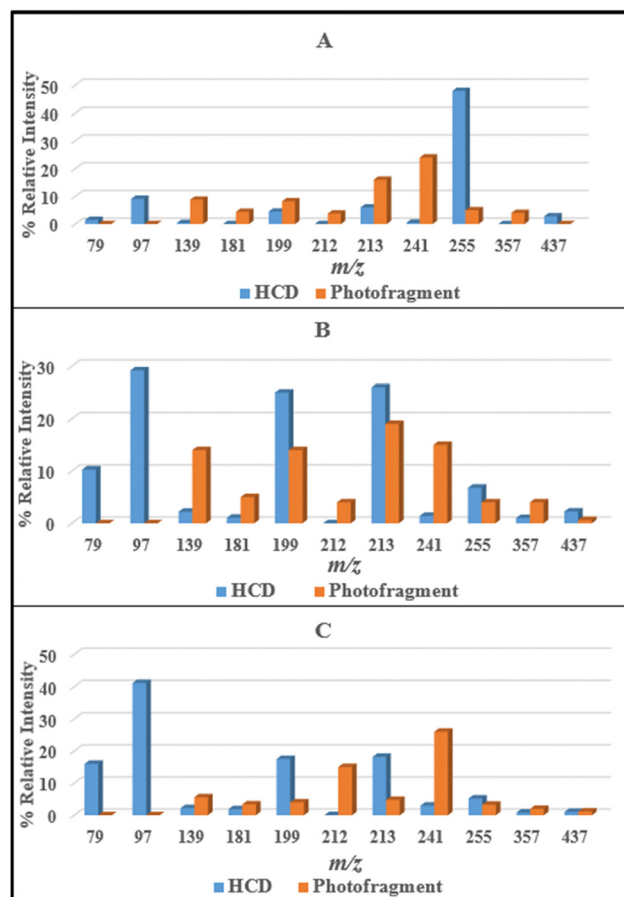

Fig. 4 Comparison of the HCD and photofragments ions produced by $[FMN-H]^-$ at (A) 8% and 3.6 eV, (B) 18% and 4.7 eV, and (C) 26% and 5.6 eV HCD energy and photon energy, respectively.

region. Strikingly, the energy channelling into the dominant HCD fragments, m/z 79 and 97, is largely minimised in the photofragmentation process, even at the highest photon energy (Fig. 4C).

Similar overall conclusions about the dominance of non-statistical decay behaviour can be drawn for the $[FMN-H]^-\cdot TRP$ and $[FMN-H]^-\cdot GLU$ complexes. For both clusters, photochemical production of the $[FMN-H]^-$ does not follow the profile of the overall photodepletion spectra (Section S2, ESI†) as would be expected if decay of the clusters was predominantly statistical. For example, both $[FMN-H]^-\cdot TRP$ and $[FMN-H]^-\cdot GLU$ show enhanced production of the m/z 213 and 241 photofragments in the lower-energy regions of band II, reflecting strong non-statistical behaviour in this region.

Fig. 5 presents a comparison of the production of the m/z 455 ($[FMN-H]^-$) fragment from HCD against the photofragment for the $[FMN-H]^-\cdot TRP$ and $[FMN-H]^-\cdot GLU$ complexes. It is only possible to present this straightforward comparison for the m/z 455 fragment for the complexes as this is the only fragment observed in HCD. Notably, the patterns of HCD *vs.* photofragmentation intensity differ for the two complexes. This reveals that distinctive photodynamics are present in the two clusters, with tryptophan binding appearing to enhance the photochemical
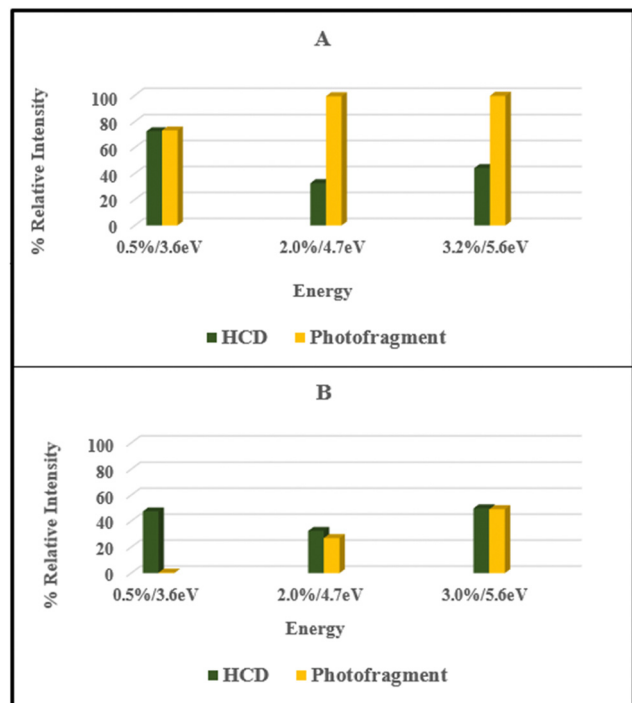
Fig. 5 Comparison of the HCD and photofragment intensities for production of the *m/z* 455 ion (*i.e.* [FMN–H]$^-$) at different % HCD and photon energy (*hν*) respectively for (A) [FMN–H]$^-$·TRP and (B) [FMN–H]$^-$·GLU.

production of the [FMN-H]$^-$ fragment compared to glutamic acid across the spectral range studied. Intriguingly, this suggests that the [FMN-H]$^-$·TRP complex is displaying photodynamics closer to statistical decay than either [FMN-H]$^-$ or [FMN-H]$^-$·GLU, consistent with TRP quenching long-lived triplet states of FMN.[51]

3.6 Comparison of the geometric structures of [FMN-H]$^-$·TRP and [FMN-H]$^-$·GLU

One of the immediate questions to be answered in understanding the differences in the photodynamics of [FMN-H]$^-$·TRP and [FMN-H]$^-$·GLU is the extent to which the two complexes are structurally distinct. Therefore, a series of calculations were performed to gain an initial insight into the clusters' geometric structures.
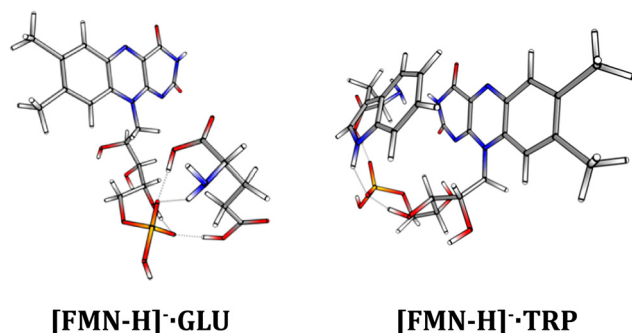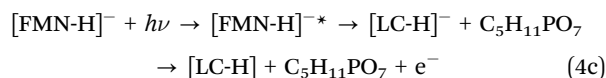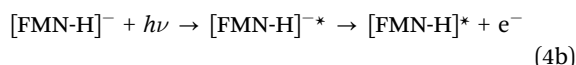

Fig. 6 The lowest-energy calculated structures of the [FMN–H]$^-$·GLU and [FMN–H]$^-$·TRP complexes. See text for details.

Fig. 6 displays the lowest-energy structures obtained for [FMN-H]$^-$·TRP and [FMN-H]$^-$·GLU clusters. Section S4 (ESI†) presents the results for other low-energy structures of the complexes. All of the calculated structures show a strong propensity to form hydrogen-bonding interactions, as expected for such gas-phase anionic molecular systems. (We note that Molano-Arevalo *et al.* have studied the gas-phase structure of the related molecule, flavin adenine dinucleotide, using ion mobility spectrometry, and obtained candidate structures using computational chemistry as part of this work.[52] Those structures incorporate similar hydrogen bonding patterns to the ones observed here.) However, comparison of the [FMN-H]$^-$·TRP and [FMN-H]$^-$·GLU lowest-energy structures shows that the two clusters display distinctive conformational preferences. While the [FMN-H]$^-$·TRP complex exhibits a preference for adopting a folded structure where the two aromatic functional groups are able to interact *via* favorable π–π interactions, the [FMN-H]$^-$·GLU cluster adopts a more open structure where the glutamic acid hydrogen bonds to the deprotonated phosphate group away from the isoalloxazine chromophore. The folded structure of [FMN-H]$^-$·TRP is notable in the context of the modified photodynamics evident for this system compared to bare [FMN-H]$^-$ and [FMN-H]$^-$·GLU and reflects TRP-flavin geometric arrangements seen in flavin proteins.[2]

4. Further discussion of the mechanism of electron detachment and excited state dynamics

Electron detachment can occur above the electron-detachment threshold of an anionic system either *via* direct detachment (4a) or indirectly from an excited state of the cluster (4b). It can also occur from hot photofragments, *e.g.* (4c). Eqn (4a)–(4c) illustrate these pathways for [FMN-H]$^-$:

$$[\text{FMN-H}]^- + h\nu \rightarrow [\text{FMN-H}] + e^- \quad (4a)$$

$$[\text{FMN-H}]^- + h\nu \rightarrow [\text{FMN-H}]^{-*} \rightarrow [\text{FMN-H}]^* + e^- \quad (4b)$$

$$[\text{FMN-H}]^- + h\nu \rightarrow [\text{FMN-H}]^{-*} \rightarrow [\text{LC-H}]^- + \text{C}_5\text{H}_{11}\text{PO}_7$$
$$\rightarrow [\text{LC-H}] + \text{C}_5\text{H}_{11}\text{PO}_7 + e^- \quad (4c)$$

The ionic fragmentation products seen following photoexcitation of [FMN-H]$^-$ and the clusters are produced with low intensities (<20% photodepletion intensity), in line with pathways (4a)–(4c) dominating decay for these flavin systems.

Wang *et al.* used anion photoelectron spectroscopy to determine that the H$_2$PO$_4^-$ anion has an adiabatic electron affinity of 4.57 eV, with a vertical detachment energy of 5.06 eV. Similarly, Nobel *et al.* have found that the adiabatic electron affinity of the phenylphosphonate anion as 4.60 eV.[44] The electron detachment energy of [FMN-H]$^-$ has not been determined to date, but would be expected to be similar to, or greater than, H$_2$PO$_4^-$ due to intramolecular hydrogen bonding stabilising the flavin anion. Similarly, the detachment energies of the

30704 | *Phys. Chem. Chem. Phys.*, 2023, **25**, 30697–30707

This journal is © the Owner Societies 2023

complexes would be likely to be higher that of the $[FMN-H]^-$ monomer as a result of intermolecular hydrogen bonding.

These considerations lead us to conclude that the direct detachment, pathway (4a), is unlikely to be important across the majority of the photoexcitation region studied here. To fully rule out decay pathways of the type illustrated in eqn (4c) would require estimates of the electron detachment energies of the possible anionic photofragments. However, from the photofragments we observe, many correspond to ions that are phosphate containing (*e.g.* $C_5H_{10}PO_7^-$), and would hence again have an associated high detachment energies that would be energetically inaccessible. This leads to the conclusion that the dominant electron loss pathway is (4b) and indicates that photoexcitation of the flavin chromophore of $[FMN-H]^-$ leads to efficient electron loss from the excited states accessed across the range 3.1–5.7 eV. While the phosphate anion displays a relatively high electron detachment of ~ 5 eV, alkoxide anions have significantly lower detachment energies of ~ 2 eV.[53] Therefore, one explanation of the strong detachment propensity observed here is that proton transfer occurs on the excited state surface of the flavin from the ribose alcohol to the phosphate group, with subsequent detachment from the resulting alkoxide. It is also possible that proton transfer occurs from the isoalloxazine group, with resulting electron detachment from the deprotonated isoalloxazine ring (detachment energy ~ 3.6 eV).[23]

Stockett and co-workers have suggested that photo-induced proton transfer occurs in the related molecule, flavin adenine dinucleotide.[25] In that work it was argued that proton transfer occurred from the isoalloxazine group to a phosphate group, although a definitive structural assignment could not be made. Taken together, the measurements on the flavin adenine dinucleotide and the systems studied here provide evidence for a strong propensity for photo-activated proton transfer in these biochemically relevant flavin molecules. In future work, it should be possible to directly probe this process using time-resolved photoelectron spectroscopy.[27,54,55] Currently there are no published photoelectron spectroscopy studies of flavin anions. Such measurements are highly desirable to determine the detachment energies and provide further key information on the coupling between photoexcitation and photodetachment.[56] They would also be important in the context of the known behaviour of lumiflavin in solution, where presolvated electrons have been observed following photoexcitation of lumiflavin under conditions where the deprotonated is present.[57]

Finally, we note that the propensity for electron detachment is equally strong for $[FMN-H]^-\cdot TRP$ and $[FMN-H]^-\cdot GLU$, as for the $[FMN-H]^-$ monomer. It is striking that complexation with the TRP and GLU amino acids does not reduce the intrinsic propensity for electron detachment from $[FMN-H]^-$, reflecting the dominance of the intrinsic chromophore dynamics.

5. Conclusions

Previous work on $[FMN-H]^-$ revealed that a substantial fraction of photoactivated ions decay by non-statistical fragmentation pathways, which occur prior to the complete conversion and redistribution of electronic excitation energy across the vibrational degrees of freedom.[17] Our studies of the $[FMN-H]^-\cdot TRP$ and $[FMN-H]^-\cdot GLU$ complexes reveal that similar non-statistical decay pathways persist upon complexation of $[FMN-H]^-$ with these amino acids. This behaviour contrasts with that of nucleobase clusters we have studied previously, where statistical photodecay pathways dominate as a result of ultrafast excited state decay by the nucleobase chromophore.[49,58] While both complexes display non-statistical decay pathways, there are clear differences in the photodynamics displayed. The $[FMN-H]^-\cdot TRP$ complex shows behavior that is closer to statistical photodissociation compared to $[FMN-H]^-\cdot GLU$, which in turn displays behavior that is closer to bare $[FMN-H]^-$. These differences in photodynamics align with structural differences between the two complexes, where $[FMN-H]^-\cdot TRP$ adopts a more closed structure due to $\pi-\pi$ stabilization between the TRP and FMN. Despite the importance of key photoredox flavin systems including cryptochromes, many questions remain in relation to their detailed mechanism of action. Within such systems, three highly conserved TRP residues occupy sites adjacent to the flavin centre and form the electron-transfer chain.[8] Over recent years, a number of model systems have been developed to simplify functional studies, including flavin-TRP dyads and flavin-TRP containing unilamella vesicles.[8,59] These approaches are challenging in terms of the synthetic techniques involved. *In vacuo* cluster studies provide an alternative approach, with the results presented herein demonstrating the potential of cluster studies for addressing aspects of flavin photodynamics as a function of proximity to selected amino acids.

Data availability

Data is available from the authors on request.

Author contributions

Conflicts of interest

The authors declare no conflict of interest.

Acknowledgements

This journal is © the Owner Societies 2023

Phys. Chem. Chem. Phys., 2023, **25**, 30697–30707 | **30705**

References

1 H. B. Gray and J. R. Winkler, *Annu. Rev. Biochem.*, 1996, **65**, 537–561.

2 J. L. Dempsey, J. R. Winkler and H. B. Gray, *Chem. Rev.*, 2010, **110**, 7024–7039.

3 L. Zanetti-Polzi, M. Aschi, A. Amadei and I. Daidone, *J. Phys. Chem. Lett.*, 2017, **8**, 3321–3327.

4 J. Zelenka, R. Cibulka and J. Roithová, *Angew. Chem., Int. Ed.*, 2019, **58**, 15412–15420.

5 N. Mataga, H. Chosrowjan, S. Taniguchi, F. Tanaka, N. Kido and M. Kitamura, *J. Phys. Chem. B*, 2002, **106**, 8917–8920.

6 B. Zhuang, U. Liebl and M. H. Vos, *J. Phys. Chem. B*, 2022, **126**, 3199–3207.

7 K. S. Conrad, C. C. Manahan and B. R. Crane, *Nat. Chem. Biol.*, 2014, **10**, 801–809.

8 S. Paul, L. Meng, S. Berger, G. Grampp, J. Matysik and X. Wang, *ChemPhotoChem*, 2017, **1**, 12–16.

9 W. D. Kumler and J. J. Eiler, *J. Am. Chem. Soc.*, 1943, **65**, 2355–2361.

10 G. Li and K. D. Glusac, *J. Phys. Chem. A*, 2008, **112**, 4573–4583.

11 E. Matthews, A. Sen, N. Yoshikawa, E. Bergström and C. E. H. Dessent, *Phys. Chem. Chem. Phys.*, 2016, **18**, 15143–15152.

12 E. Matthews and C. E. H. Dessent, *J. Phys. Chem. A*, 2016, **120**, 9209–9216.

13 R. Cercola, E. Matthews and C. E. H. Dessent, *J. Phys. Chem. B*, 2017, **121**, 5553–5561.

14 S. B. Nielsen, J. U. Andersen, J. S. Forster, P. Hvelplund, B. Liu, U. V. Pedersen and S. Tomita, *Phys. Rev. Lett.*, 2003, **91**, 048302.

15 J. C. Marcum, A. Halevi and J. M. Weber, *Phys. Chem. Chem. Phys.*, 2009, **11**, 1740.

16 G. Grégoire, H. Kang, C. Dedonder-Lardeux, C. Jouvet, C. Desfrançois, D. Onidas, V. Lepere and J. A. Fayeton, *Phys. Chem. Chem. Phys.*, 2006, **8**, 122–128.

17 L. Giacomozzi, C. Kjær, S. Brøndsted Nielsen, E. K. Ashworth, J. N. Bull and M. H. Stockett, *J. Chem. Phys.*, 2021, **155**, 044305.

18 N. G. K. Wong, J. A. Berenbeim and C. E. H. Dessent, *ChemPhotoChem*, 2019, **3**, 1231–1237.

19 R. Cercola, K. O. Uleanya and C. E. H. Dessent, *Mol. Phys.*, 2020, **118**, e1662128.

20 P. Nieto, A. Günther, G. Berden, J. Oomens and O. Dopfer, *J. Phys. Chem. A*, 2016, **120**, 8297–8308.

21 D. Müller and O. Dopfer, *J. Phys. Chem. A*, 2021, **125**, 3146–3158.

22 N. G. K. Wong, C. Rhodes and C. E. H. Dessent, *Molecules*, 2021, **26**, 6009.

23 E. Matthews and C. E. H. Dessent, *J. Phys. Chem. Lett.*, 2018, **9**, 6124–6130.

24 E. Matthews, R. Cercola and C. Dessent, *Molecules*, 2018, **23**, 2036.

25 J. N. Bull, E. Carrascosa, L. Giacomozzi, E. J. Bieske and M. H. Stockett, *Phys. Chem. Chem. Phys.*, 2018, **20**, 19672–19681.

26 M. H. Stockett, *Phys. Chem. Chem. Phys.*, 2017, **19**, 25829–25833.

27 A. Henley and H. H. Fielding, *Int. Rev. Phys. Chem.*, 2019, **38**, 1–34.

28 S. Bakels, E. M. Meijer, M. Greuell, S. B. A. Porskamp, G. Rouwhorst, J. Mahé, M.-P. Gaigeot and A. M. Rijs, *Faraday Discuss.*, 2019, **217**, 322–341.

29 E. K. Ashworth, M.-H. Kao, C. S. Anstöter, G. Riesco-Llach, L. Blancafort, K. M. Solntsev, S. R. Meech, J. R. Verlet and J. N. Bull, *Phys. Chem. Chem. Phys.*, 2023, **25**, 23626–23636, DOI: **10.1039/D3CP03250G**.

30 C. S. Anstöter, B. F. E. Curchod and J. R. R. Verlet, *Phys. Chem. Chem. Phys.*, 2022, **24**, 1305–1309.

31 W. Zagorec-Marks, L. G. Dodson, P. Weis, E. K. Schneider, M. M. Kappes and J. M. Weber, *J. Am. Chem. Soc.*, 2021, **143**, 17778–17785.

32 R. Antoine and P. Dugourd, *Phys. Chem. Chem. Phys.*, 2011, **13**, 16494.

33 T. R. Rizzo, J. A. Stearns and O. V. Boyarkin, *Int. Rev. Phys. Chem.*, 2009, **28**, 481–515.

34 E. F. Yee, S. Chandrasekaran, C. Lin and B. R. Crane, *Methods in Enzymology*, Elsevier, 2019, vol. 620, pp. 509–544.

35 R. K. Kar, A. Miller and M. Mroginski, *Wiley Interdiscip. Rev.: Comput. Mol. Sci.*, 2022, **12**, e1541.

36 Y. El Khoury, L. J. G. W. Van Wilderen and J. Bredenbeck, *J. Chem. Phys.*, 2015, **142**, 212416.

37 E. Matthews, PhD thesis, University of York, 2018.

38 Y. Ho and P. Kebarle, *Int. J. Mass Spectrom. Ion Processes*, 1997, **165–166**, 433–455.

39 F. Mohamadi, N. G. J. Richards, W. C. Guida, R. Liskamp, M. Lipton, C. Caufield, G. Chang, T. Hendrickson and W. C. Still, *J. Comput. Chem.*, 1990, **11**, 440–467.

40 T. Climent, R. González-Luque, M. Merchán and L. Serrano-Andrés, *J. Phys. Chem. A*, 2006, **110**, 13584–13590.

41 K. O. Uleanya and C. E. H. Dessent, *Phys. Chem. Chem. Phys.*, 2021, **23**, 1021–1030.

42 J. Simons, *J. Phys. Chem. A*, 2008, **112**, 6401–6511.

43 X.-B. Wang, E. R. Vorpagel, X. Yang and L. Wang, *J. Phys. Chem. A*, 2001, **105**, 10468–10474.

44 J. A. Noble, E. Marceca, C. Dedonder, I. Carvin, E. Gloaguen and C. Jouvet, *Eur. Phys. J. D*, 2021, **75**, 95.

45 E. Matthews, R. Cercola, G. Mensa-Bonsu, D. M. Neumark and C. E. H. Dessent, *J. Chem. Phys.*, 2018, **148**, 084304.

46 W.-L. Li, A. Kunin, E. Matthews, N. Yoshikawa, C. E. H. Dessent and D. M. Neumark, *J. Chem. Phys.*, 2016, **145**, 044319.

47 A. J. A. Harvey, N. Yoshikawa, J.-G. Wang and C. E. H. Dessent, *J. Chem. Phys.*, 2015, **143**, 101103.

48 R. Cercola, E. Matthews and C. E. H. Dessent, *Mol. Phys.*, 2019, **117**, 3001–3010.

30706 | *Phys. Chem. Chem. Phys.*, 2023, **25**, 30697–30707

This journal is © the Owner Societies 2023

49 A. Sen, T. F. M. Luxford, N. Yoshikawa and C. E. H. Dessent, *Phys. Chem. Chem. Phys.*, 2014, **16**, 15490.

50 B. Lucas, M. Barat, J. A. Fayeton, C. Jouvet, P. Çarçabal and G. Grégoire, *Chem. Phys.*, 2008, **347**, 324–330.

51 B. Zhuang, D. Seo, A. Aleksandrov and M. H. Vos, *J. Am. Chem. Soc.*, 2021, **143**, 2757–2768.

52 J. C. Molano-Arevalo, D. R. Hernandez, W. G. Gonzalez, J. Miksovska, M. E. Ridgeway, M. A. Park and F. Fernandez-Lima, *Anal. Chem.*, 2014, **86**, 10223–10230.

53 S. T. Stokes, J. E. Bartmess, A. Buonaugurio, Y. Wang, S. N. Eustis and K. H. Bowen, *Chem. Phys. Lett.*, 2019, **732**, 136638.

54 C. S. Anstöter, J. N. Bull and J. R. R. Verlet, *Int. Rev. Phys. Chem.*, 2016, **35**, 509–538.

55 A. Kunin and D. M. Neumark, *Phys. Chem. Chem. Phys.*, 2019, **21**, 7239–7255.

56 A. Sen, G.-L. Hou, X.-B. Wang and C. E. H. Dessent, *J. Phys. Chem. B*, 2015, **119**, 11626–11631.

57 P. F. Heelis, R. F. Hartman and S. D. Rose, *Photochem. Photobiol.*, 1993, **57**, 1053–1055.

58 A. Sen and C. E. H. Dessent, *J. Phys. Chem. Lett.*, 2014, **5**, 3281–3285.

59 Y. Oka, T. Miura and T. Ikoma, *J. Phys. Chem. B*, 2021, **125**, 4057–4066.

This journal is © the Owner Societies 2023

Phys. Chem. Chem. Phys., 2023, **25**, 30697–30707 | **30707**